Structures of two archaeal diphthine synthases: insights into the post-translational modification of elongation factor 2

Seiichiro Kishishita,[a]‡ Katsumi Shimizu,[b]‡ Kazutaka Murayama,[a] Takaho Terada,[a] Mikako Shirouzu,[a] Shigeyuki Yokoyama[b,c]* and Naoki Kunishima[b]*

[a]Protein Research Group, Genomic Sciences Center, Yokohama Institute, RIKEN 1-7-22, Suehiro-cho, Tsurumi, Yokohama 230-0045, Japan, [b]Advanced Protein Crystallography Research Group, RIKEN SPring-8 Center, Harima Institute, 1-1-1 Kouto, Sayo-cho, Sayo-gun, Hyogo 679-5148, Japan, and [c]Department of Biophysics and Biochemistry, Graduate School of Science, The University of Tokyo, 7-3-1 Hongo, Bunkyo-ku, Tokyo 113-0033, Japan

‡ These authors contributed equally to this work.

Correspondence e-mail:
yokoyama@biochem.s.u-tokyo.ac.jp,
kunisima@spring8.or.jp

The target of diphtheria toxin is the diphthamide residue in translation elongation factor 2 (EF-2), which is generated by a three-step post-translational modification of a specific histidine residue in the EF-2 precursor. In the second modification step, an *S*-adenosylmethionine-dependent methyltransferase, diphthine synthase (DS), catalyzes the trimethylation of the EF-2 precursor. The homodimeric crystal structures of the archaeal diphthine synthases from *Pyrococcus horikoshii* OT3 and *Aeropyrum pernix* K1 have been determined. These structures share essentially the same overall fold as the cobalt-precorrin-4 methyltransferase CbiF, confirming that DS belongs to the dimeric class III family of methyltransferases. In the *P. horikoshii* DS dimer, only one of the two active sites binds the reaction product *S*-adenosyl-L-homocysteine (AdoHcy), while the other active site contains no ligand. This asymmetric AdoHcy binding may be a consequence of intra-domain and inter-domain movements upon binding of AdoHcy at one of the two sites. These movements disrupt the twofold dimeric symmetry of the DS dimer and probably cause lower AdoHcy affinity at the other binding site.

1. Introduction

The diphthamide residue, 2-[3-carboxyamido-3-(trimethyl-ammonio)propyl]histidine, in translation elongation factor 2 (EF-2) is the target of diphtheria toxin. This toxin, produced by the *tox* gene in *Corynebacterium diphtheriae*, catalyzes the ADP-ribosylation of the diphthamide residue in eukaryotic and archaebacterial EF-2 (Pappenheimer, 1977; Kessel & Klink, 1980). As a result of this ribosylation, the modified EF-2 cannot perform its ribosomal function of polypeptide-chain elongation, thus leading to cell death (Wilson & Collier, 1992). In contrast to the abundance of information about ADP-ribosylation toxicity, the physiological role of the diphthamide residue in eukaryotic and archaeal cells remains obscure. However, a cryo-electron microscopy study of the yeast EF-2–ribosome complex revealed that the diphthamide-containing domain IV of EF-2 is located in the vicinity of the tRNA in the protein-biosynthetic complex (Gomez-Lorenzo *et al.*, 2000). Furthermore, the crystal structure of yeast EF-2 identified the exact location of the diphthamide residue (His699) in a solvent-exposed tip region of domain IV, which would be accessible to tRNA in the ribosome complex (Jørgensen *et al.*, 2003). These facts suggest some regulatory role of the diphthamide residue in eukaryotic and archaeal protein biosynthesis.

The diphthamide residue is generated by the post-translational modification of the specific precursor histidine in EF-2 by three modification enzymes (Moehring *et al.*, 1984). The first step of this reaction is the transfer of a 3-amino-3-carboxypropyl group from *S*-adenosylmethionine (AdoMet) to the imidazole C-2 of the specific histidine precursor residue in EF-2 (Dunlop & Bodley, 1983). After this reaction, tri-methylation of the resulting amino group follows to produce the diphthine residue, concomitant with the consumption of three AdoMet molecules and the release of three *S*-adenosyl-L-homocysteine (AdoHcy) molecules (Fig. 1). The final step is ATP-dependent amidation of the diphthine residue to form the diphthamide residue. The second trimethylation step is catalyzed by the AdoMet-dependent methyltransferase diphthine synthase (DS), which is widespread among eukaryotes and archaea but has never been found in bacteria. A sequence analysis suggested that DS belongs to the homodimeric class III family of methyltransferases (Schubert *et al.*, 2003). Here, we report the crystal structures of the diphthine synthases from the anaerobic and aerobic hyper-thermophilic archaea *Pyrococcus horikoshii* OT3 and *Aeropyrum pernix* K1, respectively (Kawarabayasi *et al.*, 1998; Sako *et al.*, 1996). These structures provide a detailed understanding of the DS architecture and insights into its conformational changes upon substrate binding.

2. Materials and methods

2.1. Protein purification

The diphthine synthase APE0931 from *A. pernix* K1 (*Ap*DS) has a molecular weight of 31.5 kDa and consists of 294 amino-acid residues. The *Ap*DS gene was amplified by PCR from genomic DNA and subcloned into the pET11a vector. A selenomethionine (SeMet) derivative of the protein was expressed in *Escherichia coli* B834 (DE3) cultured in modified LeMaster medium (Hendrickson *et al.*, 1990) and induced with isopropyl β-D-1-thiogalactopyranoside (IPTG).

The cell lysate was incubated at 343 K for 30 min and was then centrifuged to remove the denatured protein. The soluble fraction was applied onto a HiTrap Q column (Amersham Biosciences) previously equilibrated with 20 m*M* Tris–HCl buffer pH 8.0 containing 1 m*M* DTT. The eluted fraction was applied onto a HiTrap Butyl FF column (Amersham Biosciences) previously equilibrated with 20 m*M* Tris–HCl buffer pH 8.0 containing 1.2 *M* ammonium sulfate and 1 m*M* DTT. The proteins were eluted with a linear gradient of 1.2–0 *M* ammonium sulfate. The soluble fraction was desalted using a HiPrep 26/10 desalting column (Amersham Biosciences). The fraction was applied onto a Mono Q 10/100 column (Amersham Biosciences) previously equilibrated with 20 m*M* Tris–HCl buffer pH 8.0 containing 1 m*M* DTT. The proteins were eluted with a linear gradient of 0–1 *M* NaCl. The fractions containing *Ap*DS were collected, pooled and dialyzed against 20 m*M* Tris–HCl buffer pH 8.0 containing 150 m*M* NaCl and 1 m*M* DTT. Finally, the protein was applied onto a HiLoad 16/60 Superdex 75 prep-grade gel-filtration column (Amersham Biosciences) previously equilibrated with 20 m*M* Tris–HCl pH 8.0 containing 150 m*M* NaCl and 1 m*M* DTT. The purified protein was concentrated to 16.8 mg ml^{-1} using a Centricon filter (Millipore). The yield of the SeMet-substituted *Ap*DS was 12.9 mg from 4.6 g of wet cells.

The diphthine synthase from *P. horikoshii* OT3 (*Ph*DS) has a molecular weight of 29.6 kDa and consists of 265 amino-acid residues. The *Ph*DS gene was amplified by PCR from genomic DNA and subcloned into the pET11a vector. For the preparation of native *Ph*DS, *E. coli* BL21-CodonPlus (DE3)-RIL cells were transformed with the recombinant plasmid and grown at 310 K in Luria–Bertani medium containing 50 µg ml^{-1} ampicillin for 20 h. The harvested cells were disrupted by sonication and heated at 363 K for 13 min. The cell debris and denatured protein were removed by centrifugation. The crude extract was desalted with a HiPrep 26/10 desalting column (Amersham Biosciences) and applied onto a Super Q Toyopearl 650M (Tosoh) column equilibrated with 20 m*M* Tris–HCl buffer pH 8.0 (buffer *A*). After elution with a
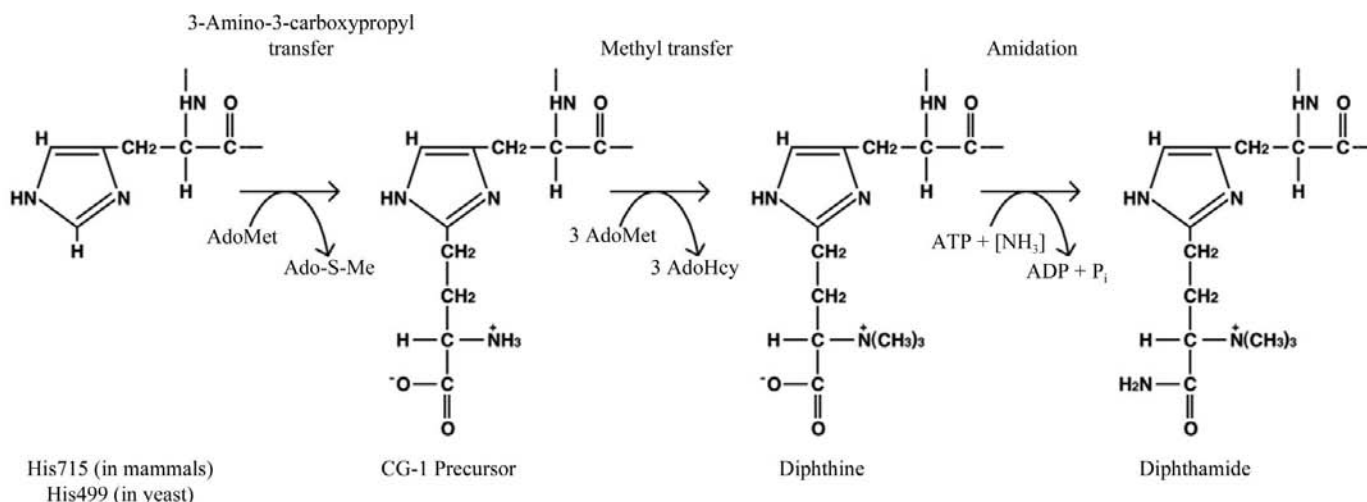
Figure 1
The overall pathway of the post-translational modification of diphthamide.

Table 1
Summary of crystallographic analysis.

Values in parentheses are for the highest resolution shell.

	*Ap*DS (Se MAD)			*Ph*DS (native)	*Ph*DS (Se SAD)
Data collection					
Radiation wavelength (Å)	0.9791	0.9794	0.9640	1.0	0.9791
Space group	$P4_12_12$	$P4_12_12$	$P4_12_12$	$P4_12_12$	$P4_12_12$
Unit-cell parameters (Å)	$a = 62.8, c = 129.7$			$a = 104.9, c = 137.3$	$a = 104.7, c = 138.6$
Measured reflections	140929	140863	140737	615733	634370
Unique reflections	18308	18320	18296	45377	45658
Resolution range (Å)	50.0–2.0 (2.07–2.00)	50.0–2.0 (2.07–2.00)	50.0–2.0 (2.07–2.00)	40.0–2.1 (2.18–2.10)	40.0–2.1 (2.18–2.10)
Completeness (%)	99.7 (100)	99.7 (100)	99.6 (100)	100 (100)	100 (100)
$I/\sigma(I)$	20.1 (7.5)	28.3 (7.9)	25.7 (7.9)	11.9 (3.7)	11.1 (3.8)
R_{merge}† (%)	7.2 (27.5)	5.9 (25.4)	6.0 (25.4)	7.4 (60.3)	6.1 (42.6)
Phasing					
Mean FOM‡ before solvent flattening		0.56			0.32
Refinement					
No. of reflections					
Working set	18308			45377	
Test set	891			2255	
Resolution range (Å)	30.5–2.0 (2.13–2.00)			39.0–2.1 (2.23–2.10)	
R factor (%)	19.9 (25.3)			19.8 (23.5)	
R_{free} (%)	24.4 (30.2)			22.8 (25.3)	
Subunits in the ASU	1			2	
No. of solvent atoms	116			446	
Average B factor (Å^2)					
Overall	40.7			36.5	
Solvent	38.5			47.8	
Ligand (AdoHcy)	—			34.1	
R.m.s.d. bond lengths (Å)	0.01			0.01	
R.m.s.d. bond angles (°)	1.7			1.4	
Estimated coordinate error (Å)	0.22			0.24	
Ramachandran plot, residues in (%)					
Most favoured region	90.2			91.8	
Allowed regions	8.9			8.2	
Generously allowed regions	0.8			0	
Disallowed regions	0			0	

† $R_{merge} = \sum_{hkl} \sum_i |I_i(hkl) - \langle I(hkl)\rangle| / \sum_{hkl} \sum_i I_i(hkl)$, where $I_i(hkl)$ is the observed intensity and $\langle I(hkl)\rangle$ is the average intensity. ‡ Mean figure of merit $= \langle |\sum P(\alpha)\exp(i\alpha)/\sum P(\alpha)| \rangle$, where α is the phase and $P(\alpha)$ is the phase probability distribution.

linear gradient of 0–0.3 *M* NaCl, the fraction containing *Ph*DS was desalted with a HiPrep 26/10 desalting column (Amersham Biosciences) using buffer *A*. The sample was fractionated on a Resource Q column (Amersham Biosciences) equilibrated with buffer *A*. After elution with a linear gradient of 0–0.3 *M* NaCl, the fraction containing *Ph*DS was desalted on a HiPrep 26/10 desalting column with 10 m*M* phosphate–NaOH buffer pH 7.0 (buffer *B*). The sample was then applied onto a Bio-Scale CHT-20-I column (Bio-Rad) equilibrated with buffer *B* and was eluted with a linear gradient of 10–150 m*M* phosphate–NaOH buffer pH 7.0. The sample was concentrated by ultrafiltration (Vivaspin, 10 kDa cutoff, Vivascience) and loaded onto a HiLoad 16/60 Superdex 200 prep-grade column (Amersham Biosciences) equilibrated with buffer *A* containing 0.2 *M* NaCl. The homogeneity and identity of the purified sample were assessed by SDS–PAGE and N-terminal sequence analysis, respectively. Finally, the purified native *Ph*DS was concentrated to 32.8 mg ml^{-1} by ultrafiltration and stored at 203 K. For the SeMet-substituted *Ph*DS, *E. coli* BL21-Codon Plus (DE3)-RIL-X cells were initially pre-cultured at 310 K for 7 h in Luria–Bertani medium containing 1.0% polypeptone, 0.5% yeast extract, 0.5% NaCl and 100 µg ml^{-1} ampicillin pH 7.0. Subsequently, the transformants were grown at 310 K overnight in SeMet

core medium containing 0.13 µ*M* L-selenomethionine, 21 types of amino acids and bases, 1% pre-mixed vitamin solution (Sigma), 1.0% lactose, 50 µg ml^{-1} ampicillin and 25 µg ml^{-1} chloramphenicol pH 7.0. The SeMet-substituted protein was purified in the same manner as the native protein and virtually identical results to those of the native protein were obtained.

2.2. Crystallization

The crystallization of SeMet-substituted *Ap*DS was performed by the hanging-drop vapour-diffusion method in Linbro plates at 293 K. For the crystallization, 1 µl protein solution (2.6 mg ml^{-1}) in 20 m*M* Tris–HCl buffer pH 8.0 containing 150 m*M* NaCl and 1 m*M* DTT was mixed with 1 µl precipitant solution containing 30.8% 2-methyl-2,4-pentanediol (MPD). Drops were equilibrated against 30% MPD precipitant solution. Typical crystal dimensions were 300 × 200 × 100 µm. Since the precipitant MPD also functions as a cryoprotectant, the crystal was cooled directly from the drops in a 93 K nitrogen stream without additional cryoprotection.

Crystals of *Ph*DS were obtained by the microbatch method using NUNC HLA plates (Nalge Nunc International). For the native sample, crystallization drops were prepared by mixing 1.0 µl precipitant solution comprising 1.8 *M* ammonium
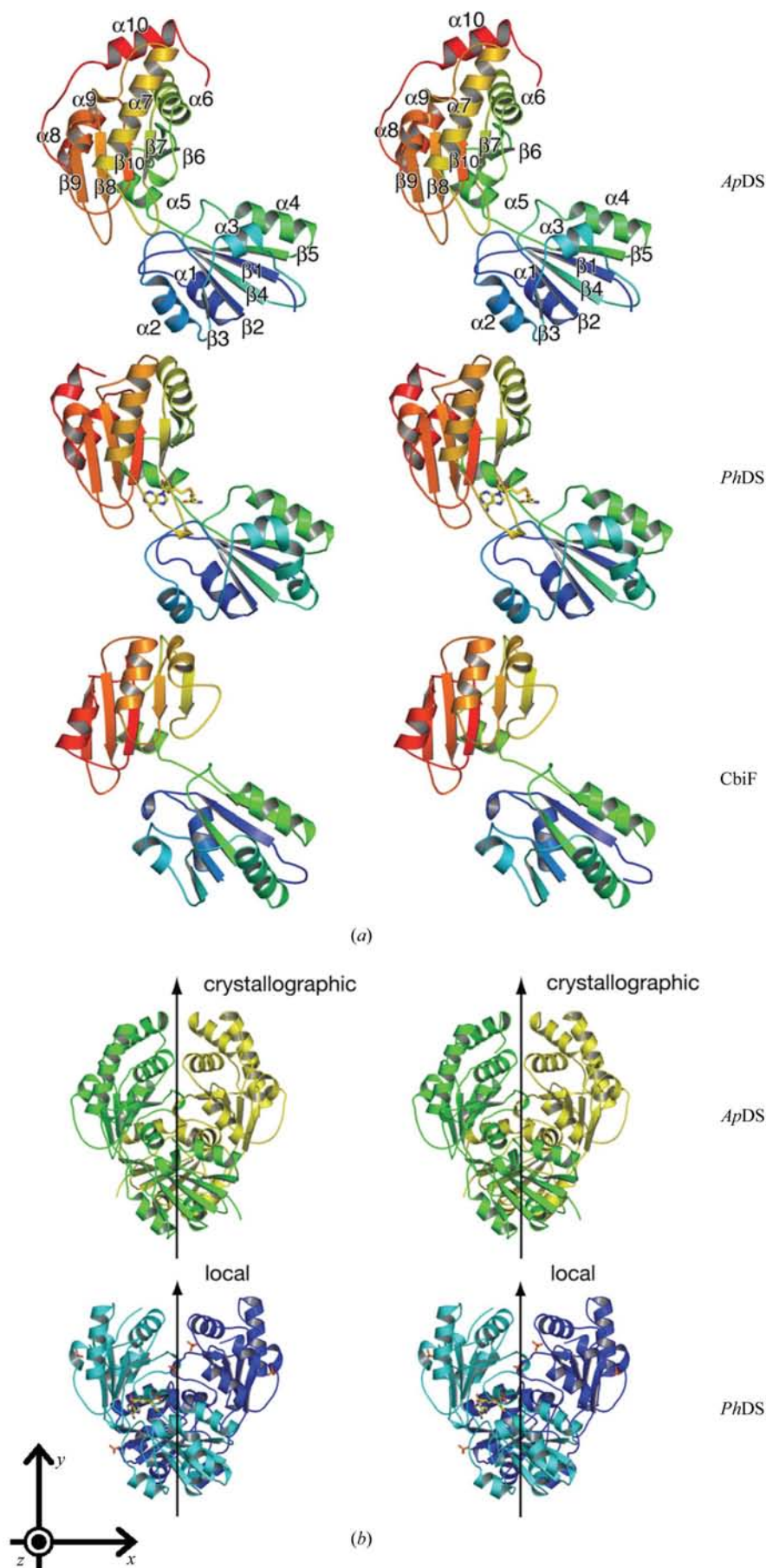
sulfate, 0.1 M MES–NaOH buffer pH 6.5 and 0.01 M cobalt chloride with 1.0 µl protein solution (32.8 mg ml⁻¹). The drops were overlaid with 15 µl of a 7:3(v:v) paraffin oil:silicone oil mixture and were incubated at 295 K. For the SeMet-substituted sample, a 0.5 µl aliquot of optimized precipitant solution comprising 3.85 M sodium formate and 0.1 M acetate–NaOH buffer pH 5.5 was mixed with 0.5 µl protein solution (25.7 mg ml⁻¹) and the drops were overlaid with 15 µl of a 7:3(v:v) paraffin oil:silicone oil mixture and incubated at 291 K. The typical crystal dimensions for both the native and SeMet-substituted crystals were 200 × 200 × 200 µm. The obtained crystals were flash-cooled in a nitrogen-gas stream at 100 K with a cryosolvent composed of 1.8 M ammonium sulfate, 0.1 M MES–NaOH buffer pH 6.5, 0.01 M cobalt chloride and 20%(v/v) glycerol for the native crystal and a cryosolvent composed of 3.85 M sodium formate, 0.1 M acetate–NaOH buffer pH 5.5 and 30%(v/v) glycerol for the SeMet-substituted crystal.

2.3. Data collection

X-ray diffraction data sets were collected at beamline BL26B1 of SPring-8, Japan (Ueno *et al.*, 2006). In order to employ the multiple anomalous dispersion (MAD) method using the SeMet-substituted *Ap*DS crystals, data sets were collected at three different wavelengths (peak, edge and high-

Figure 2
Crystal structures of diphthine synthases. (*a*) Ribbon diagrams of the subunit structures of *Ap*DS, *Ph*DS and the DS homologue CbiF. The N-terminus is coloured blue and the C-terminus is coloured red. The bound AdoHcy molecule in the *Ph*DS subunit is depicted as a stick model. The AdoHcy molecule observed in CbiF is omitted for clarity. (*b*) Stereo ribbon diagrams of the dimer structures of *Ap*DS and *Ph*DS. The subunits are coloured yellow and green in *Ap*DS and cyan and blue in *Ph*DS. In the *Ph*DS structure, six sulfate ions are present on the surface of the protein and AdoHcy is present in the active site. The crystallographic and local twofold axes of the dimeric symmetry are shown by arrows. For comparison with the other figures, the direction of the projection is shown by coordinate axes at the bottom left of the figure. The figures were generated using *PyMOL* (DeLano, 2002).

energy remote). For the single anomalous dispersion (SAD) method using the SeMet-substituted *Ph*DS crystals, a data set was collected at the peak wavelength. These data were processed and scaled using the programs *DENZO* and *SCALEPACK* (Otwinowski & Minor, 1997). The crystals belong to space group $P4_12_12$, with unit-cell parameters $a = b = 62.8, c = 129.7$ Å for *Ap*DS and $a = b = 104.9, c = 137.3$ Å for *Ph*DS (native). The data-collection statistics are presented in Table 1.

2.4. Structure determination

Since molecular-replacement phasing was not successful, we had to solve both the *Ap*DS and the *Ph*DS structures independently by experimental phasing. To obtain the electron-density map, we used the *SOLVE* program package (Terwilliger & Berendzen, 1999). For *Ap*DS, four selenium sites were found in the asymmetric unit. After density modification, an initial model was built with the program *RESOLVE* (Terwilliger, 2000). The model was built with the program *TURBO-FRODO* (Roussel & Cambillau, 1989) using the peak data. Structural refinement was performed using *CNS* (Brünger *et al.*, 1998). Finally, the crystal structure of SeMet-substituted *Ap*DS was refined at 2.0 Å resolution to R and R_{free} factors of 0.199 and 0.244, respectively (Table 1). The crystal structure of *Ph*DS was determined in a similar manner, using the 12 selenium sites observed in the asymmetric unit of the SeMet-substituted *Ph*DS crystal. Model building and revision were performed with the program *QUANTA*2000 (Accelrys Inc.). Finally, the crystal structure of native *Ph*DS was determined at 2.1 Å resolution with R and R_{free} factors of 0.198 and 0.228, respectively (Table 1).

3. Results and discussion

3.1. Overall fold

We solved the crystal structures of the diphthine synthases from *P. horikoshii* OT3 (*Ph*DS) and *A. pernix* K1 (*Ap*DS) at resolutions of 2.1 and 2.0 Å, respectively, using the multiwavelength anomalous dispersion (MAD) method (Table 1). In both structures, a kidney-shaped monomeric subunit is formed by two α/β domains linked by a hinge region. The N-terminal and C-terminal

domains contain a parallel β-sheet with 32415 topology and a mixed β-sheet with 12534 topology, respectively (Fig. 2*a*). Both of the DS crystals show similar homodimers of two subunits associated together with twofold symmetry (Fig. 2*b*). The twofold axis is crystallographic in the *Ap*DS crystal but is local in the *Ph*DS crystal; the crystallographic asymmetric unit contains a subunit in the *Ap*DS crystal, whereas it contains a dimer in the *Ph*DS crystal. In the *Ph*DS dimer, an AdoHcy
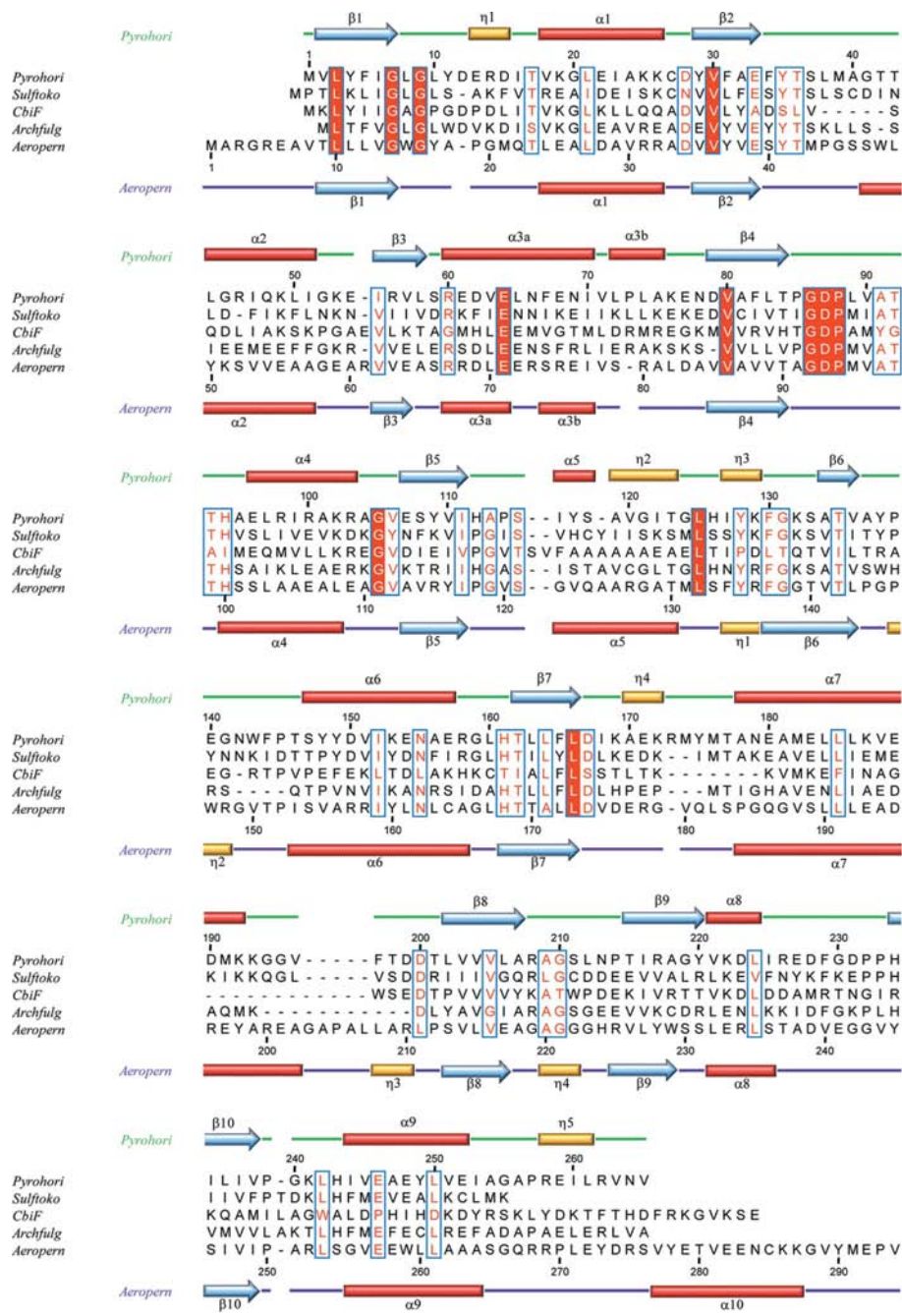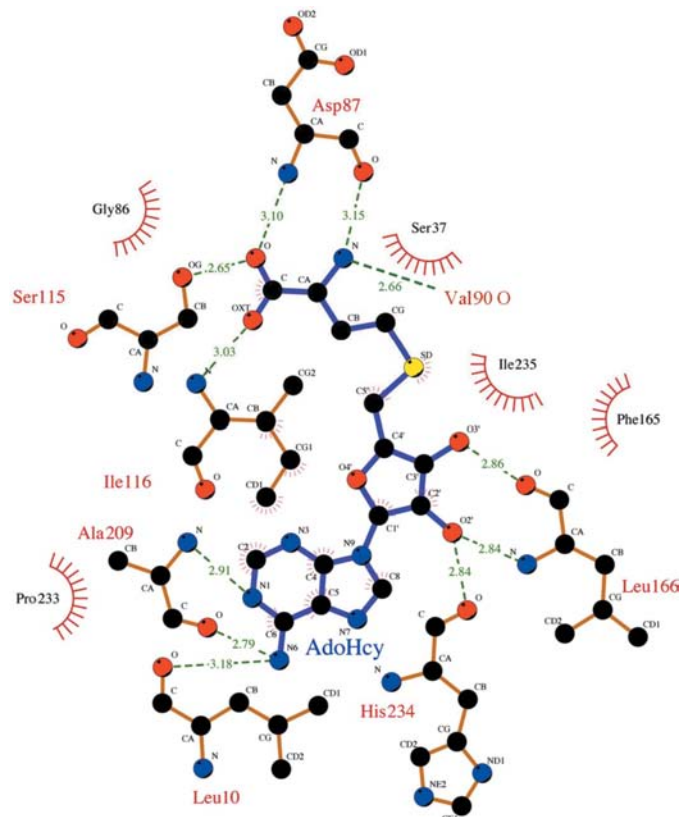

Figure 3
Multiple sequence alignments and secondary-structure assignments of diphthine synthases. Helices and strands are shown as cylinders and arrows, respectively. Conserved residues are highlighted. The labels are as follows: *Aeropern*, *Aeropyrum pernix* K1 (gi: 14601080); *Pyrohori*, *Pyrococcus horikoshii* OT3 (gi: 14590602); *Sulftoko*, *Sulfolobus tokodaii* strain 7 (gi: 15921541); *Archfulg*, *Archaeoglobus fulgidus* (gi: 40889957; PDB code 1vhv; Badger *et al.*, 2005).

molecule resides in one of the two active-site pockets and six sulfate ions are bound on the molecular surface. A structural comparison of the *Ap*DS subunit with the *A* and *B* subunits of the *Ph*DS dimer using the program *DALI* produced high
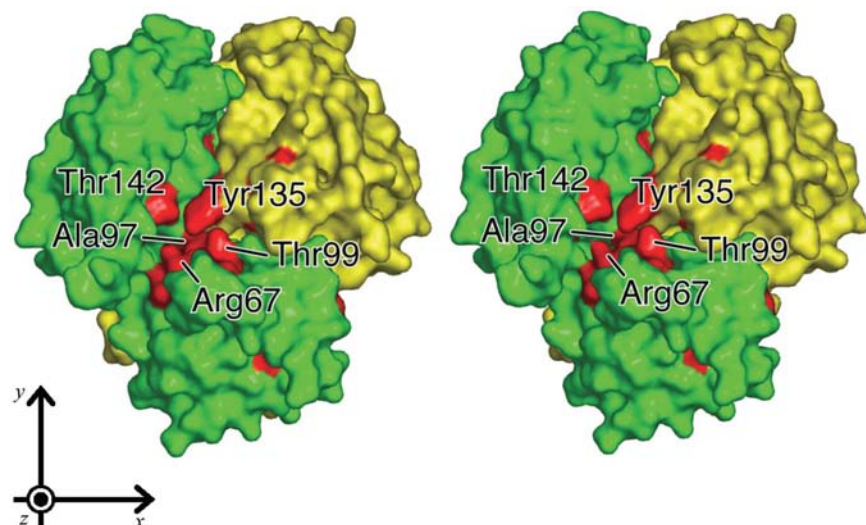

Figure 4
Representation of AdoHcy binding in *Ph*DS. This figure was generated using *LIGPLOT* (Wallace *et al.*, 1995).

Figure 5
Surface-conservation pattern of the *Ap*DS dimer. The entirely conserved residues are coloured red. Because of their overlapping, the positions of the conserved Glu71 and Asp174 residues are not shown in this figure. The subunit colouring is the same as that in Fig. 2(*b*). For comparison with the other figures, the direction of the projection is shown by coordinate axes at the bottom left of the figure. The figures were generated using *PyMOL* (DeLano, 2002).

scores: *Z* scores of 25.2 and 26.4 and root-mean-square deviation (r.m.s.d.) values of 2.4 and 2.2 Å, respectively (Holm & Sander, 1997). Thus, these *Ap*DS and *Ph*DS structures share high similarity, apart from the additional C-terminal α11 helix in *Ap*DS (Fig. 3). The *Ap*DS structure was compared with previously reported structures in the Protein Data Bank (PDB) using the program *DALI*. The crystal structure of a cobalamin-biosynthetic enzyme, cobalt-precorrin-4 methyltransferase (CbiF; Schubert *et al.*, 1998), gave high scores when compared with the *Ap*DS structure, indicating substantial structural similarity: the *Z* score was 15.9 and the r.m.s.d. was 3.5 Å (Fig. 2*a*). This result agrees well with the fact that DS and CbiF have similar main-chain folds and share the same β-sheet topology. In contrast, a *BLAST* (Altschul *et al.*, 1990) search revealed marginal sequence similarity between DS and CbiF, with *e* values for *Ap*DS and *Ph*DS against CbiF of 0.65 and 12.0, respectively. The AdoHcy-binding site is also conserved between DS and CbiF and is located on the hinge region between the N-terminal and C-terminal domains (Figs. 2*a* and 3). The AdoMet-dependent methyltransferases have been classified into five different families (classes I–V) by structural folding (Schubert *et al.*, 2003). These structural characteristics are consistent with the fact that DS and CbiF are both classified as homodimeric class III AdoMet-dependent methyltransferases.

3.2. *S*-Adenosyl-L-homocysteine-binding site

The *S*-adenosyl-L-homocysteine (AdoHcy) molecule observed within the *Ph*DS crystal structure is the physiological product of the methyl-transfer reaction. Since neither AdoHcy nor AdoMet was added during the crystallization of *Ph*DS, this endogenous AdoHcy may have been incorporated during the preparation steps. This AdoHcy appears to be bound by both hydrogen bonds and hydrophobic interactions (Fig. 4). Interestingly, of the 11 hydrogen bonds between *Ph*DS and AdoHcy, ten are mediated by peptidyl backbone N or O atoms and only one hydrogen bond, that between Ser115 O^γ and AdoHcy O, is derived from a side-chain atom. This AdoHcy-binding mode is quite similar to that observed in the CbiF crystal structure (Schubert *et al.*, 1998); of the 12 hydrogen bonds between CbiF and AdoHcy, ten and two are mediated by main-chain and side-chain atoms, respectively, and ten are equivalent to those in *Ph*DS. Some essential differences between the structures are the additional side-chain-mediated hydrogen bond between AdoHcy OXT and Ser112 O^γ in CbiF and the alternative recognition of AdoHcy O3′ by the backbone O atom of Leu166 in *Ph*DS or by the backbone N atom of Leu164 in CbiF. Hydrophobic interactions with the Pro233 and Ile116 residues also seem to contribute to the ligand

binding, as the adenosine ring of AdoHcy is sandwiched by these residues. These polar and nonpolar interactions may be important for maintaining AdoMet in the preferred position for the catalytic reaction. In the class I methyltransferases, the $O4'-C4'-C5'-S^\delta$ dihedral angle of AdoMet is around 180° (Schubert *et al.*, 2003). However, this angle is 87.6° in *Ph*DS and a similar angle (82°) for AdoHcy was observed in the CbiF structure (Schubert *et al.*, 1998). These ligand conformations, which are distinct from those in the class I enzymes, may be characteristic of the class III enzymes.

3.3. Probable EF-2-binding and catalysis modes

The *Ap*DS dimer contains two identical large clefts related by the dimeric twofold symmetry (Fig. 5). Each cleft is formed by three domains in the dimer: the N- and C-terminal domains of one subunit and the C-terminal domain of the other subunit. The AdoHcy-binding site is located at the bottom of the large cleft, which is consistent with the accommodation of EF-2. In order to evaluate the functional importance of the cleft, we mapped the conserved residues in the DS orthologues onto the molecular surface of *Ap*DS (Fig. 5). Interestingly, all of the conserved residues are aggregated on the surface of the cleft wall, suggesting their functional importance: Arg67, Glu71, Ala97 and Thr99 of the N-terminal domain, Thr142 and Asp174 of the C-terminal domain and Tyr135 of the C-terminal domain of the other subunit.

Several crystal structures of EF-2 [the first crystal structure (Jørgensen *et al.*, 2003), the ADP-ribosylated form (Jørgensen *et al.*, 2004) and the complex with a fragment of *Pseudomonas aeruginosa* exotoxin A (Jørgensen *et al.*, 2005)] have been reported. To investigate the DS active site further, we manually created a docking model of *Ph*DS with yeast EF-2 (PDB code 1n0v; Jørgensen *et al.*, 2003) containing a diphthine precursor residue (Figs. 6a and 6b). In the catalytic reaction, the diphthamide precursor His699 of yeast EF-2 must be located in the vicinity of the methyl group of AdoMet within a distance sufficient for methyl transfer. To make the docking model, we placed the S atom of AdoHcy and the diphthamide precursor residue His699 of yeast EF-2 at the preferred
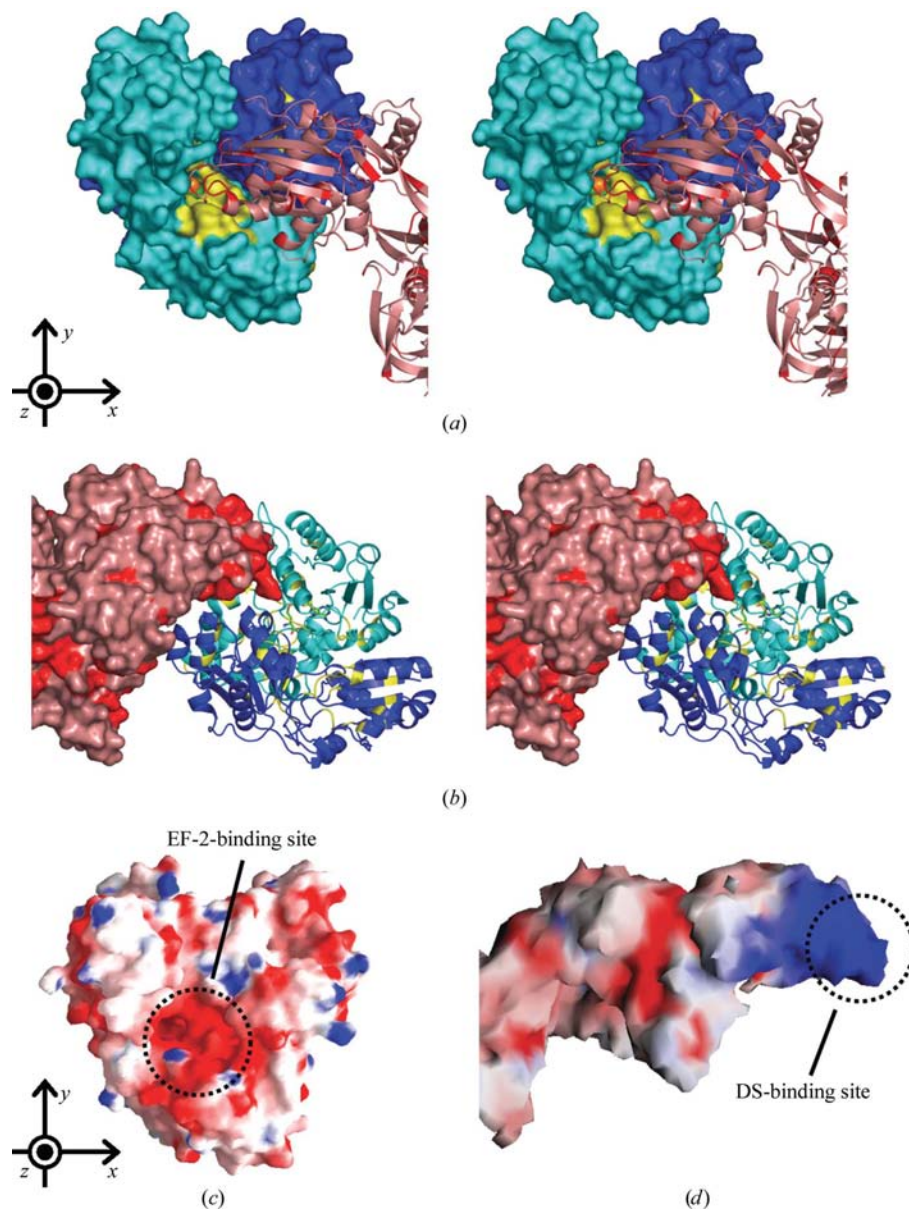
Figure 6
Putative EF-2 binding site of diphthine synthase. The docking models of *Ph*DS and yeast EF-2 are shown in (a) and (b), respectively. The subunit colouring of *Ph*DS is the same as that in Fig. 2(b). The model of yeast EF-2 is coloured salmon pink. The conserved residues are coloured yellow (*Ph*DS) and red (yeast EF-2). (a) and (b) were generated using *PyMOL* (DeLano, 2002). The electrostatic potentials of *Ph*DS and yeast EF-2 are shown in (c) and (d), respectively. The positive and negative charges are coloured blue and red, respectively. (c) and (d) were generated using *GRASP* (Nicholls *et al.*, 1991). For comparison with the other figures, the direction of the projection for (a) and (c) is shown by coordinate axes at the bottom left of each figure.

positions for the reaction and manually rotated both molecules to achieve the best fitting without steric clashes. Entirely conserved residues were observed on the surface of the docking region in both *Ph*DS and yeast EF-2, suggesting the biological relevance of this model. In the structure of *Ph*DS, the EF-2-binding site is surrounded by negatively charged residues (Fig. 6c). On the other hand, the DS-binding site of EF-2 is surrounded by positively charged residues (Fig. 6d). These electrostatic interactions, as well as the entirely conserved residues, may be important for the molecular

Table 2
C$^{\alpha}$ superposition in the *Ph*DS dimer.

The annotation of each domain is shown in the caption of Fig. 8.

Primary fitting†		Secondary fitting‡							Local shift
		Rigid-body shift							
			Rotation axis (°)		Rotation (°)				
Fitted part	R.m.s.d. (Å)	Fitted part	ω	φ	χ	Axis–centroid distance (Å)	Residue of least shift	R.m.s.d. (Å)	R.m.s.d. (Å)
D2_B_N (green)→ D1_A_N (pink)	0.55	D2_B_C (blue)→ D1_A_C (red)	127.8	94.5	3.8	18.1	Tyr128	1.40	0.92
		D2_A_C (blue)→ D1_B_C (red)	162.2	112.3	2.7	19.0	Ser118	1.04	0.92

† C$^{\alpha}$ atoms of the dimer viewed from the ligand-free side were superimposed on the dimer viewed from the ligand-bound side in the N-terminal domains. ‡ After the primary fitting, the indicated C-terminal domains of the dimers were fitted again and the applied rotations in spherical polar angle are listed. Axis–centroid distance means the distance between the rotational axis and the centroid of the subunit used in the secondary fitting. The rotational axis passes in the vicinity of the indicated residues with the least rigid-body shift. The definition of spherical polar angles is as described in Collaborative Computational Project, Number 4 (1994).

recognition of DS in the catalytic reaction. The diphthamide precursor His699 is located on domain IV in yeast EF-2 (Jørgensen *et al.*, 2003). During protein synthesis, domain IV of EF-2 is situated in the vicinity of the t-RNA in the ribosomal complex (Valle *et al.*, 2003). The highly conserved EF-2 residues around His699 may also be important for the interaction with the ribosome.

The catalytic reaction of the class III methyltransferases is thought to proceed by the S$_{N}$2 displacement of the methyl group of AdoMet. In the active site of CbiF there are no charged residues around the substrate-binding site, suggesting that the methyl-transfer reaction may be facilitated by the lability of AdoMet and the proximity and orientation of the substrate, rather than by a general acid/base mechanism (Schubert *et al.*, 1998). The docking model of *Ph*DS with yeast EF-2 revealed a hydrophobic reaction environment, in agreement with that in CbiF, suggesting that these methyltransferases share similar reaction mechanisms.

3.4. Product release

The replacement of the product, AdoHcy, with the substrate, AdoMet, is an important point in the trimethylation reaction. A single AdoMet molecule supplies only one methyl group and thus two more exchanges of AdoHcy for AdoMet occur in the active site. In the structure of *Ph*DS, the AdoHcy is at the bottom of the EF-2-binding cleft. After the methyl transfer from AdoMet to EF-2, the active-site pocket is covered by EF-2. One possibility is that another tunnel is used for exchanging AdoMet and AdoHcy. In the *Ap*DS structure, we observed a cavity extending from the active site to the surface of the DS molecule. Fig. 7 shows the structure of *Ap*DS with the superimposed structure of the product AdoHcy. This tunnel is wide enough to accommodate the adenyl ring of AdoHcy and thus may facilitate the exchange of AdoMet and AdoHcy without releasing EF-2 in *Ap*DS, although this type of tunnel was not observed in *Ph*DS. However, this tunnel is close to the end of the loop region between the α6 helix and the β7 strand. This loop may act as a gate for the AdoMet substrate and the AdoHcy product.

3.5. Implications of the dimeric state

The asymmetric unit of the *Ph*DS crystal contains two subunits: *A* and *B*. This apparent homodimeric state is consistent with the results of a dynamic light-scattering experiment, which revealed a dimeric state of *Ph*DS in solution (data not shown). The four domains from the two chains intimately associate to form the dimer interface, in which interactions between the same domains and with the cross-domains are observed. The extensive dimer interface of *Ph*DS has a buried surface area of 2550 Å^{2} per subunit, with a hydrophobic core and 25 hydrogen bonds. Interestingly, a copurified intrinsic product, AdoHcy, was only found in chain *A*, implying a differing environment around the AdoHcy-binding site.

Enzymes generally undergo conformational changes upon ligand binding. A recent study of the phenylacetate-degradation protein PaaI demonstrated subtle structural differences between several liganded and unliganded forms using the multiple C$^{\alpha}$ superposition technique (Kunishima *et al.*, 2005). In order to analyze the structural differences between the two AdoHcy-binding sites of *Ph*DS, we employed the same technique. The *Ph*DS dimer viewed from the ligand-free side (D2) was superimposed on the same dimer viewed from the ligand-bound side (D1) as a reference dimer in two steps: primary fitting and secondary fitting. In the primary fitting, the C$^{\alpha}$ atoms in the N-terminal domain (residues Met1–Ser115) of subunit *B* of dimer D2 (D2_B_N) were superimposed onto those in the N-terminal domain of subunit *A* of dimer D1 (D1_A_N) to minimize the r.m.s.d. between the two dimers. In the C-terminal domains (residues Ile116–Val265) obvious structural differences were observed, indicating substantial rigid-body shifts (Fig. 8). After the primary fitting, the superimposed C-terminal domains of subunits *B* (D2_B_C) and *A* (D2_A_C) were superimposed again onto the C-terminal domains of subunits *A* (D1_A_C) and *B* (D1_B_C), respectively (secondary fitting). The combination of an intersubunit rigid-body shift and an intrasubunit local shift can precisely describe the structural differences between the superimposed dimers.
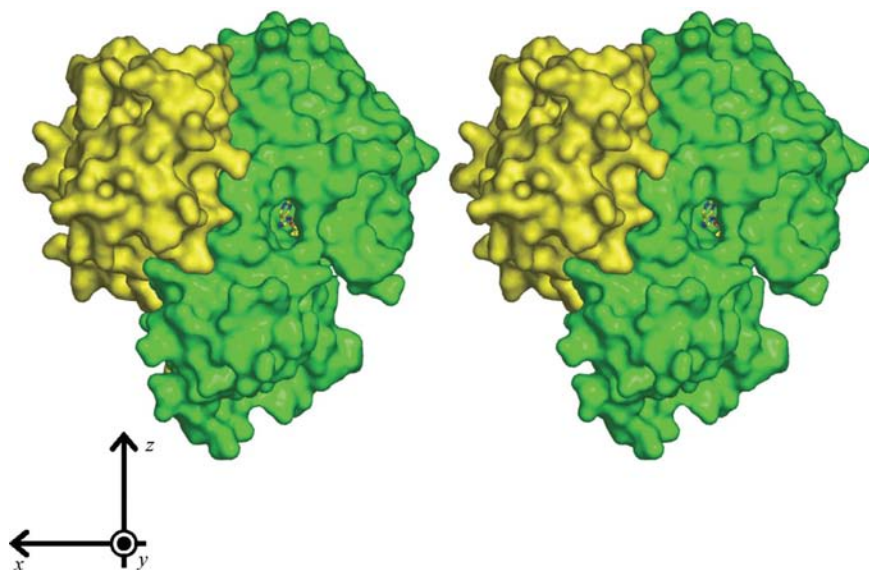
Figure 7
A ligand tunnel for effective product–substrate exchange in *Ap*DS. The subunit colouring is the same as that in Fig. 2(*b*). The putative AdoHcy molecule is depicted as a stick model, based on superposition with the *Ph*DS structure. For comparison with the other figures, the direction of the projection is shown by coordinate axes at the bottom left of the figure. This figures were generated using *PyMOL* (DeLano, 2002).
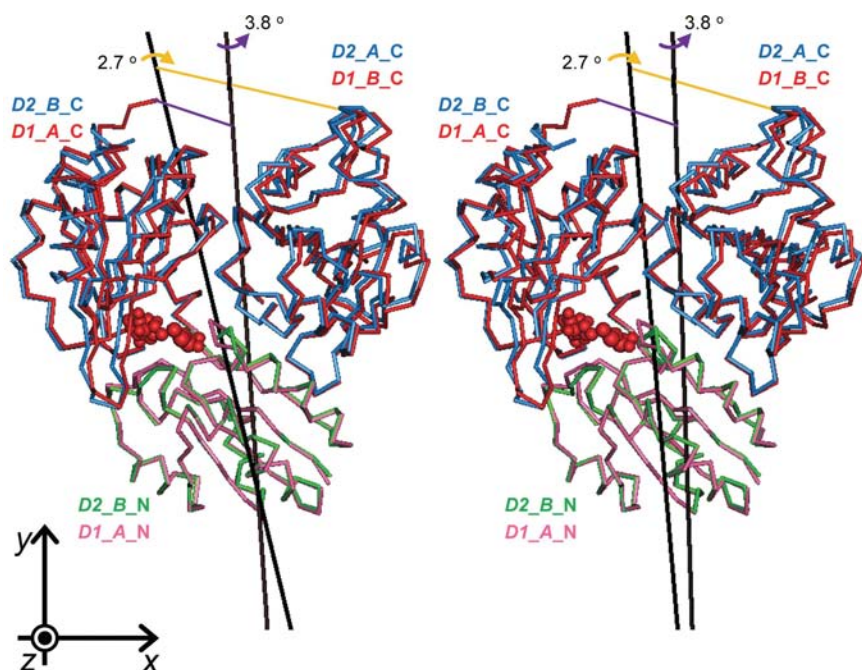
Figure 8
Rigid-body rotation of the C-terminal domains in the *Ph*DS dimer upon ligand binding. The protein C$^\alpha$ trace and the ligand AdoHcy are shown as licorice and van der Waals models, respectively. The red and pink models represent the dimer viewed from the ligand-bound side (dimer 1; *D*1) and the blue and green models represent the same dimer viewed from the ligand-free side (dimer 2; *D*2). The annotation of each domain is indicated as (dimer name)_(chain name)_(domain name) with the colour code. Two N-terminal domains (*D*1_*B*_N and *D*2_*A*_N) are omitted for clarity. The rotational axes of the C-terminal domains in the secondary fitting (Table 2) are depicted as thick black lines with purple and orange arrows and lines that represent the direction of rotation and the affiliation to the relevant C-terminal domain, respectively. For comparison with the other figures, the direction of the projection is shown by coordinate axes at the bottom left of the figure. The superposition was carried out using *LSQKAB* (Collaborative Computational Project, Number 4, 1994). This figure was generated using *QUANTA*2000 (Accelrys Inc.).

A summary of the C$^\alpha$-superposition analysis of *Ph*DS is shown in Table 2. For the local shift in the primary fitting, the r.m.s.d. value of 0.55 Å is smaller than that of 0.92 Å in the secondary fitting. This is a consequence of the large structural differences in the flexible C-terminal residues: the local shift r.m.s.d. value for the secondary fitting becomes 0.37 Å when residues Glu259–Val265 are excluded. Thus, a comparison of the r.m.s.d.s between the rigid-body and local shifts reveals that the rigid-body r.m.s.d. is generally larger than the local r.m.s.d., suggesting the major contribution of rigid-body shifts to the conformational change upon ligand binding. This agrees with the fact that most of the hydrogen bonds involved in AdoHcy recognition are mediated by main-chain atoms. The secondary fitting revealed long distances between the rotational axis and the centroid, indicating that the rigid-body shifts can be recognized as hinge motions rather than simple rotations at the centroid. Importantly, the rotation axes of the rigid-body shifts are approximately aligned with the twofold dimeric axis of the *Ph*DS dimer. This arrangement of the rotation axes tends to break the twofold symmetry of the *Ph*DS dimer and probably causes low AdoHcy affinity at the other binding site.

4. Conclusion

Trimethylation and the recognition of a large substrate are among the interesting characteristics of the DS enzyme. DS must load AdoMet (a methyl-group donor) at the bottom of the active site and has to recognize another large substrate, EF-2. After the methyl-transfer reaction, DS has to eject the product, AdoHcy, from the bottom of the active site. Thus, each reaction transfers only one methyl group and DS performs this turnover three times for the trimethylation of the diphthamide in EF-2. The structural information on *Ap*DS and *Ph*DS allowed us to propose a possible model of the catalytic turnover. The structure of *Ap*DS represents the starting structure of the catalytic turnover of DS. In the next step, the substrate AdoMet is bound to the active site of DS. The structure of *Ph*DS, which contains the product AdoHcy, revealed the intersubunit and intrasubunit shifts. These shifts may be introduced by the binding of the substrate AdoMet. The reported crystal structure of

CbiF has the same molecular architecture as that of DS, except that the CbiF dimer symmetrically binds two AdoHcy molecules (Schubert *et al.*, 1998). Thus, the ligand-binding symmetry in CbiF is disrupted in DS. CbiF is thought to catalyze the methylation of cobalt-precorrin-4 to generate cobalt-precorrin-5 in the anaerobic biosynthesis of vitamin B$_{12}$. The larger substrate size of EF-2 (MW > 90 kDa) compared with that of precorrin may account for this difference in the ligand binding. The asymmetry observed in the *Ph*DS dimer might be important for the effective recognition of a large protein substrate, in which three domains from both of the subunits in the dimer asymmetrically recognize a single EF-2 molecule.

References

Altschul, S. F., Gish, W., Miller, W., Myers, E. W. & Lipman, D. J. (1990). *J. Mol. Biol.* **215**, 403–410.

Badger, J. *et al.* (2005). *Proteins*, **60**, 787–796.

Brünger, A. T., Adams, P. D., Clore, G. M., DeLano, W. L., Gros, P., Grosse-Kunstleve, R. W., Jiang, J.-S., Kuszewski, J., Nilges, M., Pannu, N. S., Read, R. J., Rice, L. M., Simonson, T. & Warren, G. L. (1998). *Acta Cryst.* D**54**, 905–921.

Collaborative Computational Project, Number 4 (1994). *Acta Cryst.* D**50**, 760–763.

DeLano, W. L. (2002). *The PyMOL Molecular Graphics System.* DeLano Scientific, San Carlos, USA.

Dunlop, P. C. & Bodley, J. W. (1983). *J. Biol. Chem.* **258**, 4754–4758.

Gomez-Lorenzo, M. G., Spahn, C. M. T., Agrawal, R. K., Grassucci, R. A., Penczek, P., Chakraburtty, K., Ballesta, J. P. G., Lavandera, J. L., Garcia-Bustos, J. F. & Frank, J. (2000). *EMBO J.* **19**, 2710–2718.

Hendrickson, W. A., Horton, J. R. & LeMaster, D. M. (1990). *EMBO J.* **9**, 1665–1672.

Holm, L. & Sander, C. (1997). *Nucleic Acids Res.* **25**, 231–234.

Jørgensen, R., Merrill, A. R., Yates, S. P., Marquez, V. E., Schwan, A. L., Boesen, T. & Andersen, G. R. (2005). *Nature (London)*, **436**, 979–984.

Jørgensen, R., Ortiz, P. A., Carr-Schmid, A., Nissen, P., Kinzy, T. G. & Andersen, G. R. (2003). *Nature Struct. Biol.* **10**, 379–385.

Jørgensen, R., Yates, S. P., Teal, D. J., Nilsson, J., Prentice, G. A., Merrill, A. R. & Andersen, G. R. (2004). *J. Biol. Chem.* **279**, 45919–45925.

Kawarabayasi, Y. *et al.* (1998). *DNA Res.* **5**, 147–155.

Kessel, M. & Klink, F. (1980). *Nature (London)*, **287**, 250–251.

Kunishima, N., Asada, Y., Sugahara, M., Ishijima, J., Nodake, Y., Sugahara, M., Miyano, M., Kuramitsu, S., Yokoyama, S. & Sugahara, M. (2005). *J. Mol. Biol.* **352**, 212–228.

Moehring, T. J., Danley, D. E. & Moehring, J. M. (1984). *Mol. Cell. Biol.* **4**, 642–650.

Nicholls, A., Sharp, K. A. & Honig, B. (1991). *Proteins*, **11**, 281–296.

Otwinowski, Z. & Minor, W. (1997). *Methods Enzymol.* **276**, 307–326.

Pappenheimer, A. M. Jr (1977). *Annu. Rev. Biochem.* **46**, 69–94.

Roussel, A. & Cambillau, C. (1989). *TURBO-FRODO. Silicon Graphics Geometry Partner Directory*, p. 81. Silicon Graphics, Mountain View, USA.

Sako, Y., Nomura, N., Uchida, A., Ishida, Y., Morii, H., Koga, Y., Hoaki, T. & Maruyama, T. (1996). *Int. J. Syst. Bacteriol.* **46**, 1070–1077.

Schubert, H. L., Blumenthal, R. M. & Cheng, X. (2003). *Trends Biochem. Sci.* **28**, 329–335.

Schubert, H. L., Wilson, K. S., Raux, E., Woodcock, S. C. & Warren, M. J. (1998). *Nature Struct. Biol.* **5**, 585–592.

Terwilliger, T. C. (2000). *Acta Cryst.* D**56**, 965–972.

Terwilliger, T. C. & Berendzen, J. (1999). *Acta Cryst.* D**55**, 849–861.

Ueno, G., Kanda, H., Hirose, R., Ida, K., Kumasaka, T. & Yamamoto, M. (2006). *J. Struct. Funct. Genomics*, **7**, 15–22.

Valle, M., Zavialov, A., Sengupta, J., Rawat, U., Ehrenberg, M. & Frank, J. (2003). *Cell*, **114**, 123–134.

Wallace, A. C., Laskowski, R. A. & Thornton, J. M. (1995). *Protein Eng.* **8**, 127–134.

Wilson, B. A. & Collier, R. J. (1992). *Curr. Top. Microbiol. Immunol.* **175**, 27–41.